Modelling the Effects of Dark Matter Minihalos in Caustic Lensing

A report detailing the work done under
the supervision of Nikita Blinov
in the summer of 2024
related to microlensing

By

Cristiano Sampaio

Table of Contents

Abstract

This project aims to construct code to examine the magnification fluctuation behaviour of caustic lensing due to randomly distributed dark matter (DM) clumps, referred to as “minihalos”. This report begins with an introduction to the physics behind gravitational lensing as well as the techniques used to solve the lens equation in this project, including inverse ray shooting and the Taylor expansion of the Fermat potential in the lens equation.

The report continues to discuss the implementation of minihalos for a given power spectrum and outlines the results and success of this project. With some adjustments, this code can be used to model the effects of various DM density profiles on different lens models.

Introduction

The most integral equation to this research is known as the lens equation. This equation characterizes the deflection of light due to the effects of gravity and its effects on images, as shown in Figure 1. The lens equation comes in various forms, such as

$$\boldsymbol{\beta} = \boldsymbol{\theta} - \boldsymbol{\alpha}(\boldsymbol{\theta}), \tag{1}$$

where $\boldsymbol{\beta}$ and $\boldsymbol{\theta}$ are the angular positions of the source and the deflected source respectively and $\boldsymbol{\alpha}$ is the deflection angle between the source's position and the observed position. Due to the high nonlinearity of this equation (as the deflection angle depends on $\boldsymbol{\theta}$), it is quite difficult to solve, as often there are no analytic solutions, outside of a few cases.

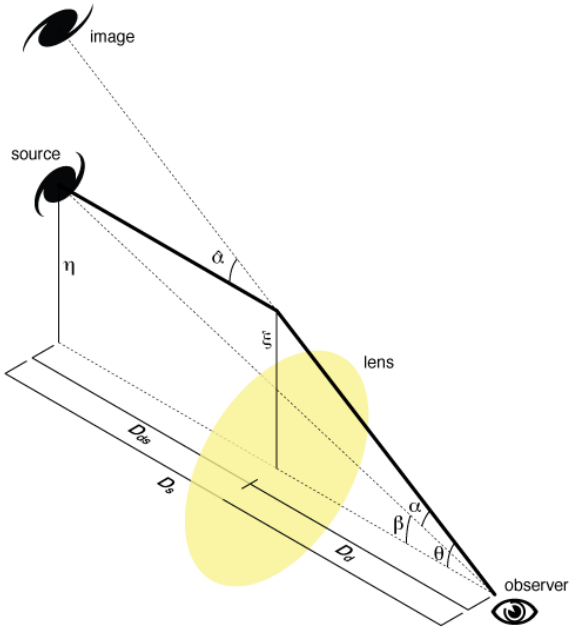

Figure 1: Illustration of the effects of gravitational lensing. An observer perceives a galaxy at a different position due to the gravitational presence of an object (in yellow) bending the light from the original position of the galaxy [1].

The technique used to perform the lensing calculations is referred to as "inverse ray shooting" (IRS), where numerous light rays are shot back from the image plane (lens plane) to the source plane, as shown in Figure 2 below. IRS is a useful, numerical method used to solve the lens equation for complex situations that also allows the generation of accurate magnification maps. The algorithm for the IRS technique is as follows:

1. Divide both the image and source plans into cells and pixels.
2. A pixel in the image plane has a ray shot back to the source plane. The deflection angle of the ray is computed.
3. The deflected ray is mapped to the source plane using the calculated deflection angle.

4. Repeat Steps 2 and 3 for each pixel.
5. Compute the total magnification using the ratio of the fluxes on the image plane and source plane. Rays that are mapped back onto the source attribute to the flux observed on the image plane.

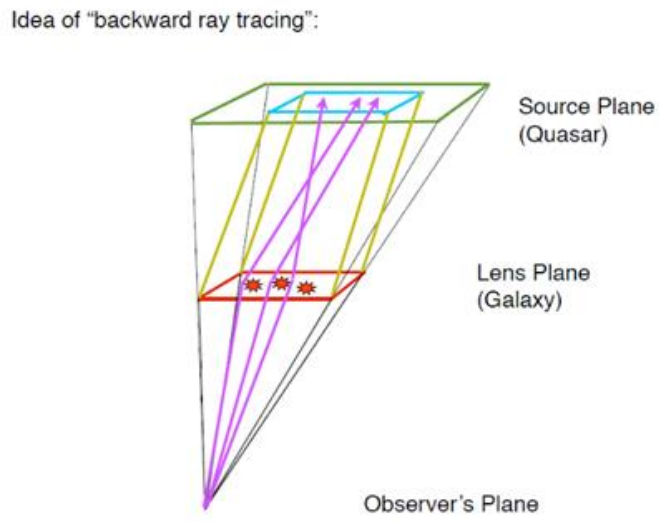

Figure 2: Diagram of inverse ray shooting, also referred to as "backward ray tracing" [2].

As outlined in the tutorial, the method to determine the magnification $\mu(x)$ was by taking the ratio of the areas of the source plane and image plane. This is possible as we are using angular coordinates in this project [2]. The code for the inverse ray shooting can be found in the Github repository labelled Array_lensing_method.py. As for the magnification mapping, that can be found under magmap.py [3]. Using these two files, you may compare with Jorge's original graphs by substituting the correct parameters as needed.

Implementation

The process for executing this project was as follows:

1. Successfully implement the inverse ray shooting program for a simple lens
2. Calculate the magnification map
3. Implement the lensing potential and the modified lens equation
4. Add stochastic fluctuations and generate plots

Quite some time was eaten during Step 1 and 2 of the process. The exact methods used to implement IRS were structured around Jorge Vicente's "Tutorial on Inverse Ray Shooting", which supplied the foundation of the created code. [2] For clarity, the code provided in the tutorial was both broken and incorrect; numerous lines were edited (especially the mapping of coordinates to pixels [4]), however the original inspiration can still be seen. Furthermore, the techniques in Jorge's tutorial were verified by calculating the magnification maps using the

inverse of the determinant of the A matrix, which is the Jacobian of the mapping $\boldsymbol{\beta}(\boldsymbol{\theta})$. Ultimately, it was made clear that the technique of using the ratio of the area of the planes had identical results and was additionally computationally faster than computing the many determinants.

To explain the procedure in step 3, we instead look at the alternate form of the lens equation:

$$\nabla_\theta \left(\frac{1}{2}(\boldsymbol{\theta}-\boldsymbol{\beta})^2 - \psi(\boldsymbol{\theta})\right) = 0 \tag{2}$$

which uses the effective lensing potential, ψ, and the fermat potential, ϕ, defined as

$$\psi(\boldsymbol{\theta}) = \frac{1}{\pi} = \int d^{\,2}\,\theta' \kappa(\boldsymbol{\theta}') \ln|\boldsymbol{\theta}-\boldsymbol{\theta}'|\,,$$
$$\phi \equiv \tfrac{1}{2}(\boldsymbol{\theta}-\boldsymbol{\beta})^2 - \psi(\boldsymbol{\theta}), \tag{3}$$

Respectively, such that the lens equation reads as follows:

$$\nabla_\theta \phi = 0 \tag{4}$$

We can further simplify this equation by Taylor expanding the Fermat potential around $\boldsymbol{x}^{(0)}$ and $\boldsymbol{y}^{(0)}$. The result is

$$\phi \approx \phi^{(0)} + \frac{1}{2}\boldsymbol{y^2} - \boldsymbol{x}\cdot\boldsymbol{y} + \frac{1}{2}\boldsymbol{x^2} + \left(\boldsymbol{x}^{(0)} - \boldsymbol{y}^{(0)}\right)\cdot(\boldsymbol{x}-\boldsymbol{y}) - \psi_1^{(0)}x_1 - \psi_2^{(0)}x_2$$
$$-\tfrac{1}{2}\psi_{11}^{(0)}x_1^2 - \tfrac{1}{2}\psi_{22}^{(0)}x_2^2 - \psi_{12}^{(0)}x_1x_2 + \ \ldots \tag{5}$$

We can further simplify this expansion by restricting our area of interest. As we are interested in regions near the caustic, we assume that the expansion point lies on the caustic. This enforces the restriction on the derivatives of the Fermat potential given that

$$0 = \det A_{ij}^{(0)} = \det \phi_{ij}^{(0)} \ \Rightarrow\ \phi_{11}\phi_{22} - \phi_{12}^2 = 0, \tag{6}$$

Which tells us $A_{ij}^{(0)}$ has at least one zero eigenvalue. Using the fact that $A_{ij}^{(0)}$ is a real symmetric matrix, it can be diagonalized using a coordinate rotation so that it reads:

$$A_{ij}^{(0)} = \begin{bmatrix} \phi_{11} & 0 \\ 0 & \phi_{22} \end{bmatrix} \tag{7}$$

such that ${\phi_{12}}^{(0)} = -{\psi_{12}}^{(0)} = 0$. We considered the simpler case where only one of these eigenvalues are 0 (specifically ${\phi_{22}}^{(0)}$), which corresponds to a “fold” caustic. The requirement of having at least one zero eigenvalue provides us with another condition on the lensing potential,

$$1 - {\psi_{22}}^{(0)} = 0\,, \tag{8}$$

where if we had chosen to set $\phi_{11}^{(0)} = 0$, it would instead be ${\psi_{11}}^{(0)}$ in the above equation. Our final constraints to simplify the Fermat expansion arise from $\boldsymbol{x}^{(0)}$ and $\boldsymbol{y}^{(0)}$ satisfying the lens equation:

$$0 = \phi_i^{(0)} = x_i^{(0)} - y_i^{(0)} - \psi_i^{(0)}. \tag{9}$$

We can now further simplify the Fermat potential as

$$\phi \approx \phi^{(0)} + \tfrac{1}{2}\boldsymbol{y^2} - \boldsymbol{x}\cdot\boldsymbol{y} + \tfrac{1}{2}\phi_{11}^{(0)}x_1^{\boldsymbol{2}} + \tfrac{1}{2}\phi_{22}^{(0)}x_2^{\boldsymbol{2}} + \tfrac{1}{6}\phi_{111}^{(0)}x_1^3 + \tfrac{1}{6}\phi_{222}^{(0)}x_2^3 + \tfrac{1}{2}\phi_{112}^{(0)}x_1^{\boldsymbol{2}}x_2 + \tfrac{1}{2}\phi_{122}^{(0)}x_1x_2^2. \tag{10}$$

We finally arrive at the lens mapping

$$\begin{aligned} y_1 &= \tfrac{x_1^2\phi_{111}}{2} + x_1x_2\phi_{112} + x_1\phi_{11} + \tfrac{x_2^2\phi_{122}}{2}, \\ y_2 &= \tfrac{x_1^2\phi_{112}}{2} + x_1x_2\phi_{122} + x_2\phi_{22} + \tfrac{x_2^2\phi_{222}}{2}. \end{aligned} \tag{11}$$

These equations are used in Step 2 of IRS.

After successfully implementing the lensing near a fold caustic, we looked at adding a term, $\delta\boldsymbol{\alpha}$, to represent small-scale fluctuations from randomly distributed minihalos. This stochastic fluctuation contributes to the deflection angle such that

$$\boldsymbol{\alpha} = \boldsymbol{\alpha}_S + \delta\boldsymbol{\alpha}, \tag{12}$$

where $\boldsymbol{\alpha}_S$ is the smooth component of the lensing deflection that we've already handled. The added deflection term has the relation

$$\delta\boldsymbol{\alpha} = \tfrac{1}{\pi}\int d^2x'\,\delta\kappa(\boldsymbol{x'})\,\tfrac{\boldsymbol{x}-\boldsymbol{x'}}{|\boldsymbol{x}-\boldsymbol{x'}|^2}, \tag{13}$$

where $\delta\kappa$ are fluctuations in the lensing convergence, which can be modelled by a 2D Gaussian random field. The Fourier transformation, $\delta\kappa(\boldsymbol{l})$, are random numbers drawn from a Gaussian distribution with a given variance. The sampling procedure is

$$\delta\kappa(l) \sim \tfrac{1}{\sqrt{2\pi P_k(l)}}\exp\left(-\tfrac{\delta\kappa(l)^2}{2P_k(l)}\right), \tag{14}$$

Where the variance, $P_k(l)$, is the power spectrum. [5] By changing this parameter, we can examine the effects of varying density profiles of dark matter. In order to add the fluctuations from minihalos, Bruno Sciolla's code for generating random Gaussian fields from was modified

with the desired power spectrum [6]. The power spectrum used in this project is shown in Figure 3 below.

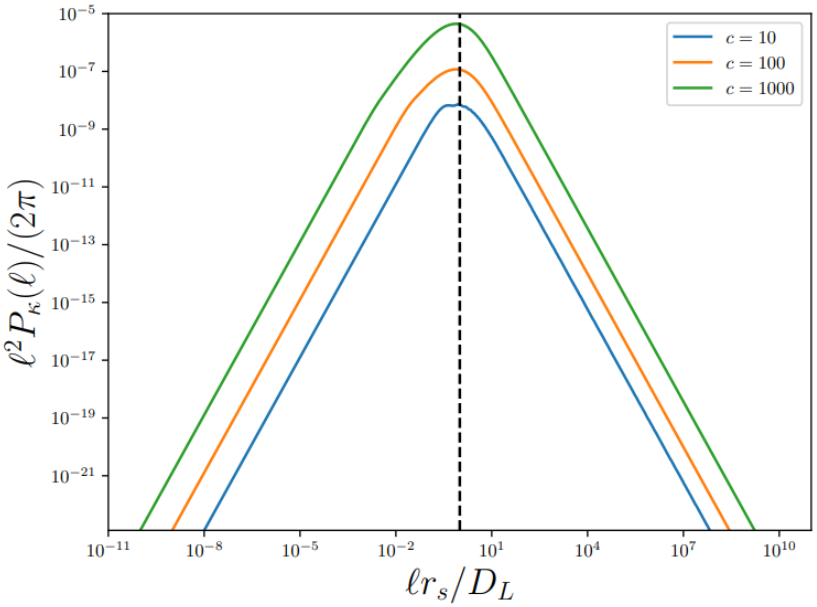

Figure 3: Convergence power spectrum used in this project. It is assumed that DM is composed of DM minihalos of equal mass with an NFW density profile [5].

After sampling a Gaussian with the given power spectrum variance, using the relation below, the Fourier transform of the stochastic fluctuation term was then calculated and inverted:

$$\delta\boldsymbol{\alpha}(\boldsymbol{l}) = \frac{2i\boldsymbol{l}}{l^2}\delta\kappa(l), \tag{15}$$

This generated the necessary stochastic fluctuations which was added to the smooth component of the lensing, as shown in (12) [5].

After the implementation of the influence of DM minihalos, the IRS technique was looped to generate the total magnification over varying vertical angular distances between a Gaussian source and the fold caustic. Plots were generated with and without the small-scale fluctuations to demonstrate their effects. These were plotted alongside the analytic solution,

$$\mu(y_c) = \sqrt{\frac{g}{R}}\xi\left(\frac{y_c}{R}\right), \tag{16}$$

where R is the radius of the source, y_c is the angular separation between the centre of the source and the caustic and g is a proportionality constant, which was derived to be

$$g = \frac{2}{\phi_{11}^2 * \phi_{222}}. \tag{17}$$

Lastly, the function $\xi\left(\frac{y_c}{R}\right)$ has the expression

$$\xi(w) = \frac{\int_w^\infty \frac{ds}{\sqrt{s-w}} \int_0^\infty dt\, f(\sqrt{s^2+t^2})}{\pi \int_0^\infty dt\, f(s)}, \tag{18}$$

where the function f(s) depends on the brightness distribution [7]. An analytic expression for (18) for a Gaussian brightness profile was used to compare with the results of the code to compare and identify any issues with the program, which can be seen in Figure 4 [8].

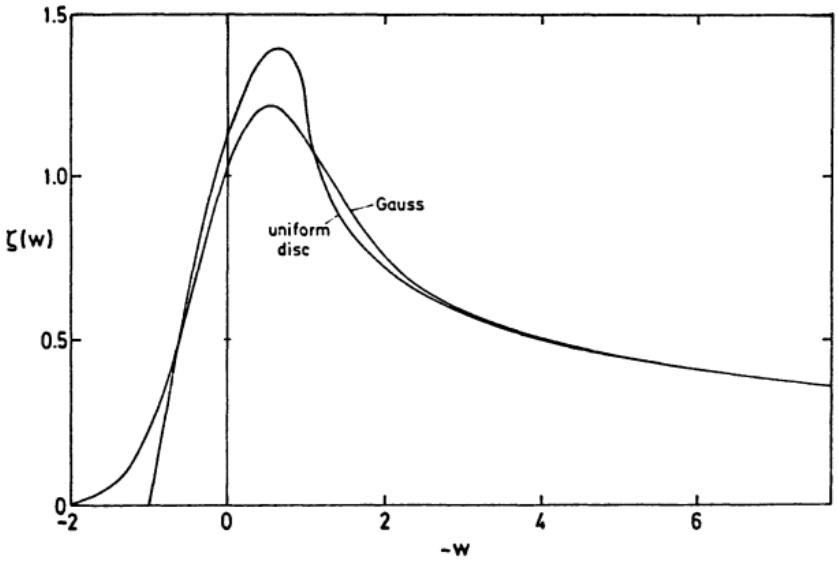

Figure 4: Magnification curve for a Gaussian source and a uniform disc relative to the angular distance of the source and the caustic [7]

Results

The implementation of the IRS technique was a success, and various cases were verified to ensure the accuracy of the code. Although the rest of the project used Gaussian sources, the use of other sources, such as a singular isothermal sphere should not be an issue with regards to the IRS code. Figure 5 provides a comparison between the plots from the code created for this project (above) and Jorge's IRS tutorial (below).

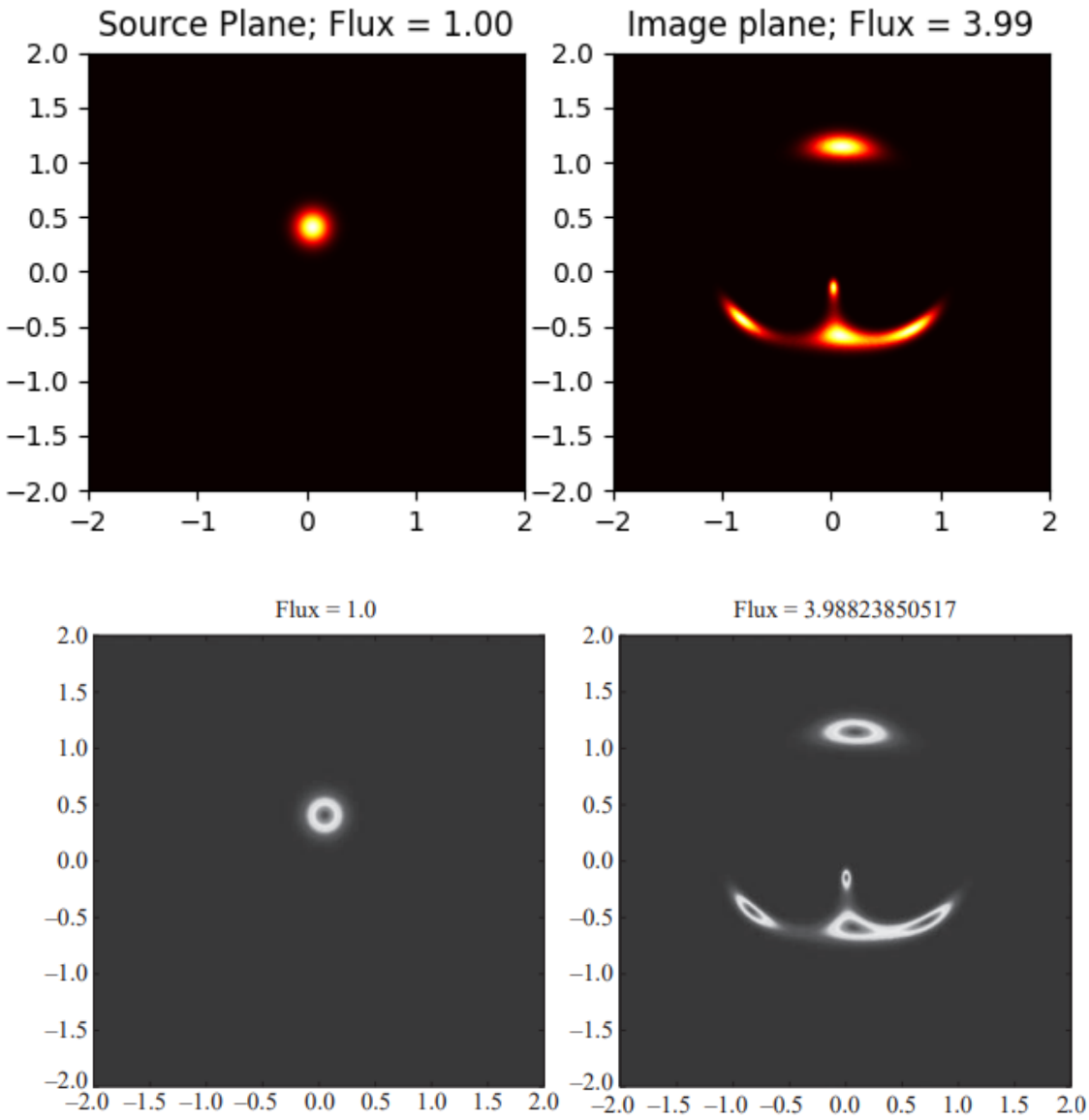

Figure 5**:** Comparison of Magnification maps of binary point of lenses of mass 0.5 positioned at (0.5,0) and (-0.5,0). Source is a circular Gaussian source positioned at (0.05,0.4) [2], [3].

Furthermore, the ability to produce code to solve the lens equation that depends on the matter distribution in the lens was mostly a success; the final magnification plot shown in Figure 6 is fairly similar to the expected curves illustrated in Figure 4, however there are some discrepancies which suggest the program requires some further adjustments, as outlined in the Ongoing Issues section. The effects of the stochastic fluctuations can be seen in green and the magnification plot with only the smooth component of the deflection angle is shown in solid blue.

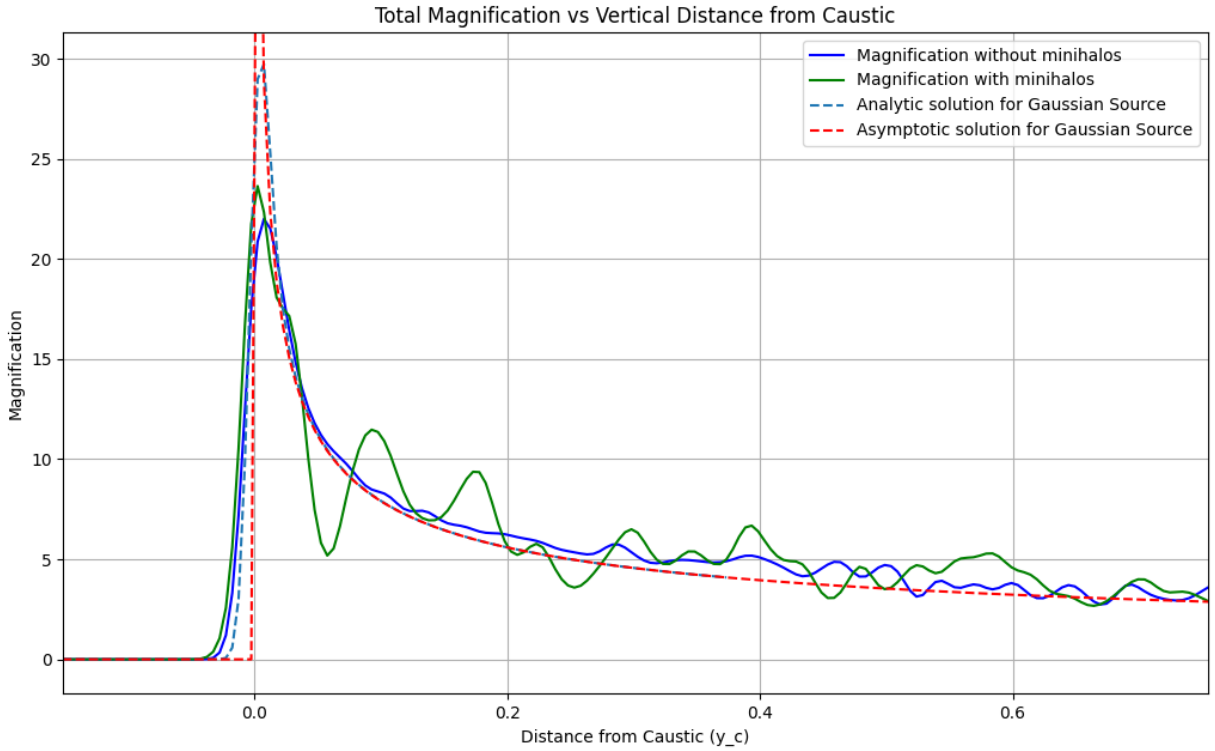

Figure 6: Magnification plotted versus the varying vertical distance of the Gaussian source from the caustic. Parameters chosen for this plot are identical to those in the repository [3].

Ongoing Issues

The magnification curve based on the distance of a Gaussian source from a caustic leaves room for improvement. As illustrated with the plots provided above, the calculations performed by the code do not entirely match with the asymptotic solution. Although the results follow the $\frac{1}{\sqrt{x}}$ behaviour for large x, it appears a constant may be missing in the calculations, as it seems the calculated curve has an overall greater magnification than the analytic solution.

Additionally, near the peak at y_{pos} = 0, where the source lies on the caustic, the magnification of the calculated curve is considerably lower than the asymptotic solution. The exact cause of this is unknown, however it was noted that changing the resolution (the number of pixels in each plane) and increasing the radius of the source shortened the gap between the asymptotic peak and the calculated peak. Attempts to fix this included examining the Fourier transformation and power spectrum in the generation of the stochastic fluctuations, but no solution was found.

Concluding Remarks

For any advancements to the existing code, It is strongly suggested to address the problems outlined earlier in this report before continuing to expand on the work. Secondly, if other sources wish to be considered, the analytic expressions of (18) will need to be implemented, as it was only considered for Gaussian sources. The examination of the Gaussian random field sampling may also be warranted, as that is where the desired power spectrum is placed.

References

[1] Sachs, M (2008) Gravitational Lensing Angles [https://commons.wikimedia.org/wiki/File:Gravitational-lensing-angles.png]

[2] Jimenez-Vicente, J. (2016). 8. Tutorial on inverse ray shooting. *Astrophysical Applications of Gravitational Lensing*, *24*, 251.

[3] Sampaio, C (2024) Lensing [https://github.com/CSampaio101/Lensing]

[4] Blinov, N. (2024) Gravitational Lensing Pixel Map

[5] Blinov, N. (2024) Tractable Lensing Models for Testing IRS

[6] Sciolla, B (2017). Gaussian Random Fields [https://github.com/bsciolla/gaussian-random-fields]

[7] Schneider, P., Ehlers, J., & Falco, E. E. (1992). *Gravitational lenses*. Springer International Publishing.

[8] Schneider, P., & Weiss, A. (1987). A gravitational lens origin for AGN-variability? Consequences of micro-lensing. *Astronomy and Astrophysics (ISSN 0004-6361), vol. 171, no. 1-2, Jan. 1987, p. 49-65.*, *171*, 49-65.